Inorg. Chem. **2007**, *46*, 9808–9818

Archetypical Modeling and Amphiphilic Behavior of Cobalt(II)-Containing Soft-Materials with Asymmetric Tridentate Ligands

Rajendra Shakya,[†] Sarmad Sahiel Hindo,[†] Libo Wu,[‡] Marco M. Allard,[†] Mary Jane Heeg,[†] Hrant P. Hratchian,[§] Bruce R. McGarvey,[||] Sandro R. P. da Rocha,[‡] and Cláudio N. Verani*,[†]

Department of Chemistry, Wayne State University, Detroit, Michigan 48202, Department of Chemical Engineering, Wayne State University, Detroit, Michigan 48202, Department of Chemistry, Indiana University, Bloomington, Indiana 47405, and Department of Chemistry and Biochemistry, University of Windsor, Windsor, ON N9B 1P4, Canada

Received June 16, 2007

The stabilization of a bivalent oxidation state in cobalt complexes of phenolate-based asymmetric tridentate ligands with iodo and bromo substituents is studied. The complexes $[Co^{II}(L^{IA})_2]\cdot 2CH_3OH$ (**1**) and $[Co^{II}(L^{BrA})_2]\cdot CH_3OH$ (**2**) were characterized by means of several spectroscopic and spectrometric techniques. The molecular structure of **1** was determined by diffractometric analysis and reveals the cobalt(II) ion in a distorted-octahedral geometry. The centrosymmetric metal ion adopts a local D_{2h} symmetry and is surrounded by facially coordinated ligands. Equivalent donor sets in both ligands are trans to each other, and DFT calculations suggest that the fac–trans configuration is favored by a small margin when compared to the fac–cis isomers. Both DFT calculations and EPR spectroscopy agree with a high-spin $S = {}^3/_2$ electronic configuration given by $[a_g^1, b_{1g}^1, a_g^1, b_{2g}^2, b_{3g}^2]$. This oxidation state was indirectly observed by the lack of a $p\pi_{phenolate} \rightarrow d\sigma^*_{cobalt(III)}$ charge-transfer band, which is found between 430 and 470 nm for similar cobalt(III) species. On the basis of the geometrical preferences and the oxidation state of archetypical **1** and **2**, two metallosurfactants $[Co^{II}(L^{I-ODA})_2]$ (**3**) and $[Co^{II}(L^{I-NOBA})_2].CH_2Cl_2$ (**4**) were obtained. The redox chemistry of **1**–**4** is marked by metal- and ligand-centered activity with several follow up processes and film formation on the electrode. Both metallosurfactants exhibit amphiphilic properties and organization, as shown by compression isotherms and Brewster angle microscopy but exhibit dissimilar collapse mechanisms; whereas **3** collapses at constant pressure, **4** exhibits a constant-area collapse. Langmuir–Blodgett films are readily obtained and were characterized by equilibrium contact angle and atomic force microscopy.

Introduction

The incorporation of transition metals to soft matter is receiving increasing interest due to potential uses toward responsive materials.[1−4] These materials are composed of a functional fragment attached to a ligand capable of coordinating metals, and their self-assembling properties facilitate the preparation of highly ordered extended structures and films. Macrocycles,[5,6] functionalized terpyridines,[7] and other symmetrical alkylpyridyl moieties with equivalent donors have been used as building blocks for cobalt(II) dendrimer-based transistors,[8] responsive ruthenium and osmium polymers,[9] multistimuli lanthanide-based plastics,[10] and metal−peptide bioconjugates.[11−13]

* To whom correspondence should be addressed. Email: cnverani@chem.wayne.edu, Phone: 313 577 1076, Fax: 313 577 8022.
[†] Department of Chemistry, Wayne State University.
[‡] Department of Chemical Engineering, Wayne State University.
[§] Department of Chemistry, Indiana University.
[||] Department of Chemistry and Biochemistry, University of Windsor.

(1) Talham, D. R. *Chem. Rev.* **2004**, *104*, 5479.
(2) Griffiths, P. C.; Fallis, I. A.; Chuenpratoom, T.; Watanesk, R. *Adv. Colloid Interface Sci.* **2006**, *122*, 107.
(3) Domonguez-Gutierrez, D.; Surtchev, M.; Eiser, E.; Elsevier, C. J. *Nano Lett.* **2006**, *6*, 145.
(4) (a) Blasini, D. R.; Flores-Torres, S.; Smilgies, D.−M.; Abruña, H. D. *Langmuir* **2006**, *22*, 2082. (b) Storrier, G. D.; Takada, K.; Abruña, H. D. *Langmuir* **1999**, *15*, 872.
(5) Bowers, J.; Danks, M. J.; Bruce, D. W. *Langmuir* **2003**, *19*, 292.
(6) Fujigaya, T.; Jiang, D.-L.; Aida, T. *J. Am. Chem. Soc.* **2003**, *125*, 14690.
(7) Schubert, U. S.; Hofmeyer, H.; Newkome, G. R. *Modern Terpyridine Chemistry*; Wiley-VCH: Weinheim, Germany, 2006.
(8) Park, J.; Pasupathy, A. N.; Goldsmith, J. I.; Chang, C.; Yaish, Y.; Petta, J. R.; Rinkoski, M.; Sethna, J. P.; Abruna, H. D.; McEuen, P. L.; Ralph, D. C. *Nature* **2002**, *417*, 722.
(9) Hjelm, J.; Handel, R. W.; Hagfeldt, A.; Constable, E. C.; Housecroft, C. E.; Forster, R. J. *Inorg. Chem.* **2005**, *44*, 1073.

10.1021/ic7011815 CCC: $37.00
Published on Web 10/17/2007

Scheme 1

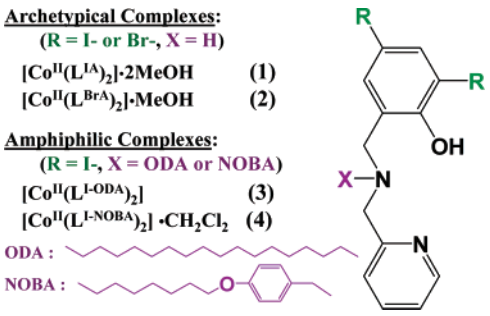

Moving toward asymmetric chelators with dissimilar donor sets[14] enables us to impart unique optical, magnetic, and redox responses leading to a broader role for metal-containing soft materials (McSM) as smart materials. Scrupulous selection of responsive donor sets and a thorough understanding of the coordination modes are pivotal for the accountability and reproducibility of these systems and may lead to improved activity. However, because the use of asymmetries increases the complexity of the approach, the design of systems based on asymmetric tridentate ligands remains largely unexplored. We are interested in redox-responsive asymmetric McSMs in which one of the donors is a phenol moiety. Phenols can be deprotonated, forming negatively charged phenolates that have the ability to form phenoxyl radicals upon oxidation. Coupling between the radical and the metal center leads to ground state switching and, therefore, to magnetic response. Phenolates also support optical responsiveness, depending on the presence or absence of ligand-to-metal charge-transfer bands related to the nature and oxidation state of the metal.

Our group has demonstrated that the mesogenic compound $[Co^{III}(L^{tBuLC})_2]ClO_4$ can generate phenoxyl radicals and that a series of $[Co^{III}(L^{RA})_2]ClO_4$ complexes with asymmetric tridentate ligands containing *tert*-butyl, methoxy, nitro, and chloro groups occupying the fourth- and sixth- positions of a phenolate ring can model successfully its coordination sphere.[15] Excellent consistency between the geometric, optical, and redox trends of the soft material and its archetypes was achieved. In this series, chloro-substituted phenolates are capable of stabilizing the quasi-reversible formation of phenoxyl radicals, so that we decided to study other halogen-substituted counterparts. Interestingly, we have observed that the iodo and bromo-substituted phenolate groups of the tridentate ligands HL^{BrA} and HL^{IA} are capable of stabilizing bivalent cobalt ions, thus forming the compounds $[Co^{II}(L^{BrA})_2]$ (**1**) and $[Co^{II}(L^{IA})_2]$ (**2**). We envisioned the development of McSMs based on such ligands, and in this article, we present the chemistry of **1** and **2** and their analogous metallosurfactants $[Co^{II}(L^{I-ODA})_2]$ (**3**) and $[Co^{II}(L^{I-NOBA})_2]\cdot CH_2Cl_2$ (**4**), in which octadecyl (OD) and nonyloxybenzyl (NOB) are functionalities incorporated to the secondary amine (A) of the archetypical ligands (Scheme 1). These metallosurfactants have potential as precursors for ordered responsive Langmuir−Blodgett films.

Experimental Section

Materials and Methods. All of the reagents were used as received from commercial sources. Methanol was dried using calcium hydride, and dichloromethane was doubly purified using alumina columns in an Innovative Technologies solvent purification system. Infrared spectra were measured from 4000 to 400 cm^{-1} as KBr pellets on a Bruker Tensor 27 FTIR spectrophotometer. ^1H NMR spectra were measured using a Varian 400 MHz instrument. ESI (positive) spectra were measured in a Micromass Quattro LC triple quadrupole mass spectrometerm, and experimental assignments were simulated for peak position and isotopic distribution. Elemental analyses were performed by Midwest Microlab: Indianapolis, Indiana. Visible spectroscopy from 1.0×10^{-4} dichoromethane solutions were performed using a Cary 50 spectrometer in the range of 250 to 1100 nm. Cyclic voltammetry experiments were performed using a BAS 50W potentiometer. A standard three-electrode-cell was employed with a glassy-carbon working electrode, a platinum-wire auxiliary electrode, and a Ag/AgCl reference electrode under an inert atmosphere at room temperature. Potentials are plotted versus Ag/AgCl and presented versus Fc^+/Fc.[16] First derivative X-Band EPR spectra of 1.0×10^{-3} M acetone solutions of **1** and **2** were performed with a Bruker ESP 300 spectrometer, using liquid helium as the coolant.

X-ray Structural Determination for 1. Crystals appeared as amber triangular rods, and a sample approximately $0.2 \times 0.15 \times 0.15$ mm^3 was used for data collection. Diffraction data were measured on a Bruker X8 APEX-II kappa geometry diffractometer with Mo radiation and a graphite monochromator. Frames were collected at 100 K as a series of sweeps with the detector at 40 mm and 0.3 degrees between each frame and were recorded for 5 s. A total of 3007 frames were collected yielding 28 555 reflections, of which 5898 were independent. *APEX-II* and *SHELX-97* software[17,18] were used in the collection and refinement of the models. Hydrogen positions were placed in observed positions. The cobalt atom occupies a crystallographic inversion center. The asymmetric unit consists of one-half of the cobalt complex and one methanol solvate.

Electronic Structure Calculations. The B3LYP/6-31G(d) level of theory[19] was employed throughout, and all of the calculations were done using the *Gaussian* series of programs.[20] Geometries were fully minimized, without symmetry constraints, using standard methods.[21] Located stationary points were characterized by computing analytic vibrational frequencies. Reported energies include zero-

(10) (a) Rowan, S. J.; Beck, J. B. *Faraday Discuss.* **2005**, *128*, 43; (b) Beck, J. B.; Rowan, S. J. *J. Am. Chem. Soc.* **2003**, *125*, 13922.
(11) Mandon, D.; Nopper, A.; Litrol, T.; Goetz, S. *Inorg. Chem.* **2001**, *40*, 4803.
(12) Storr, T.; Sugai, Y.; Barta, C. A.; Mikata, Y.; Adam, M. J.; Yano, S.; Orvig, C. *Inorg. Chem.* **2005**, *44*, 2698.
(13) (a) Kirin, S. I.; Dübon, P.; Weyhermüller, T.; Bill, E.; Metzler-Nolte, N. *Inorg. Chem.* **2005**, *44*, 5405; (b) Kirin, S. I.; Happel, C. M.; Hrubanova, S.; Weyhermüller, T.; Klein, C.; Metzler-Nolte, N. *Dalton Trans.* **2004**, 1201.
(14) (a) García-Tojal, J.; Donnadieu, B.; Costes, J. P.; Serra, J. L.; Lezama, L.; Rojo, T. *Inorg. Chim. Acta* **2002**, *333*, 132. (b) Scarpellini, M.; Neves, A.; Bortoluzzi, A. J.; Vencato, I. Drago, V.; Ortiz, W. A.; Zucco, C. *J. C. S. Dalton Trans.* **2001**, 2616. (c) Casella, L.; Gullotti, M.; Pintar, A.; Messori, L.; Rockenbauer, A.; Gyor, M. *Inorg. Chem.* **1987**, *26*, 1031. (d) Burrows, R. C.; Bailar, J. C., Jr. *J. Am. Chem. Soc.* **1966**, *88*, 4150.
(15) Shakya, R.; Imbert, C.; Hratchian, H. P.; Lanznaster, M.; Heeg, M. J.; McGarvey, B. R.; Allard, M.; Schlegel, H. B.; Verani, C. N. *Dalton Trans.* **2006**, 2517.
(16) Gagne, R.; Koval, C.; Licenski, G. *Inorg. Chem.* **1980**, *19*, 2854.
(17) *APEX II*; Bruker AXS Inc.: Madison WI, USA.
(18) Sheldrick, G., *SHELX-97*, University of Göttingen: Göttingen, Germany, 1997.

point correction. Cartesian coordinates of all of the optimized structures are provided in the Supporting Information.

Compression Isotherms and LB Films. Langmuir isotherms were measured in an automated KSV 200 minitrough at 23 ± 0.5 °C. In all of the experiments, Ultrapure water (Barnstead NANO pure) was used with a resistivity of 17.5−18 MΩ·cm^{-1}. Any impurities from the surface of freshly poured aqueous subphase were removed by vacuum, after the compression of the barriers. Spreading solutions of a known concentration (1.0 mg·mL^{-1}) were prepared in spectra grade chloroform, and a known quantity (typically 30 μL) was then spread on the clean aqueous subphase. The system was allowed to equilibrate for ca. 20 min before monolayer compression. The Π versus A compression isotherms were obtained at a compression rate of 10 mm·min^{-1}. The pressure was measured using the Wilhelmy plate method (paper plates 12 × 8 mm^2). At least three independent measurements were carried out per sample with excellent reproducibility attained. The films were transferred onto 40 × 20 × 0.08 mm^3 mica substrates (Ted Pella, Inc) at different target pressures.

Brewster Angle Microscopy. A KSV-Optrel BAM 300 with a HeNe laser (10mW, 632.8 nm) and a CCD detector was used in all of the micrographs. The compression rate was 5 mm/min, the field of view was 800 × 600 microns, and the lateral resolution was about 1 μm.

Contact Angle Measurements. The static contact angle of the substrates was determined to examine the quality of the deposited layers. The contact angle was determined on a KSV CAM 2000 goniometer equipped with a CCD camera. All of the data were collected at room temperature.

Atomic Force Microscopy. The surface topography of the LB films on fused silica substrates was examined using a Molecular Image Corp PicoSPM LE atomic force microscope using the tapping mode operation. A BS-Multi 75 silicon cantilever was used.

Synthesis of the Ligands. The archetypical ligands HL^{IA} and HL^{BrA} were synthesized as described in the literature.[15,22] The ligands HL^{I-ODA} and HL^{I-NOBA} were synthesized as follows:

The Organic Precursor 2,4-Di-iodo-6-(chloromethyl)phenol, I−CMP. 3,5 diiodosalicylaldehyde (1.87 g, 5.0 mmol) in 70 mL MeOH solution was reduced with $NaBH_4$ (0.29 g, 8.0 mmol) at 0 °C. After stirring the solution at the room temperature for 2 h, the solvent was removed and the crude product was dissolved in water. Diluted HCl (1M) was added dropwise, precipitating the solid 3,5 diiodobenzyl alcohol at pH ∼5.0. The alcohol is extracted with dichloromethane and dried over Na_2SO_4. Thionyl chloride (0.50 g, 5.0 mmol) is added to a solution of the alcohol (1.12 g, 3.0 mmol) in 80 mL dichloromethane. After 2 h at room temperature, the solvent was removed and the crude product was isolated as a brownish powder. Yield 92%. IR (KBr, cm^{-1}) 1451(s) (C═C_{ar}); 1264 (s) (C−O); ^{1}H− NMR [400 MHz, $CDCl_3$, 300K] δ/ppm = 4.60, [2x s 2x 1H (CH_2)]; 7.60 [s,1 H (aryl)]; 7.90 [s, 1 H (aryl)] ESI pos. in MeOH m/z = 493.8 for $[HL-H^+]^+$.

The Ligand 2,4-Diiodo-6-((octadecyl(pyridin-2-ylmethyl)amino)methyl)phenol, HL^{I-ODA}. Pyridine carboxyaldehyde (1.07 g, 10 mmol) was treated with octadecyl-1-amine (2.69 g, 10 mmol) in methanol at 50 °C for 1 h, yielding a yellow solution. $NaBH_4$ (0.55 g, 15 mmol) was added slowly at 0 °C. The resulting solution was stirred for 2 h at room temperature, when the solvent was removed and the crude product was extracted with 3 × 50 mL dichloromethane. The combined extracts were dried over $MgSO_4$, and the product was isolated by evaporation of the solvent. The resulting amine (1.8 g, 5 mmol) and Et_3N (1.4 mL, 10 mmol) were refluxed for 24 h in 50 mL dichloromethane in the presence of 2,4-di-iodo-6-(chloromethyl)phenol (1.97 g, 5 mmol). After completion, the product was washed with 4 × 30 mL of 5% $NaHCO_3$, and the organic layer was dried over $MgSO_4$. Upon solvent evaporation, an oil-like product was obtained and later recrystallized in acetone to give an off-white powder. Yield: 75%. IR (KBr, cm^{-1}) 2850(s), 2914(s) (alkyl− CH−); 1593(m), 1541(m) ,1452(s) (C═N_{py}, C═C_{ar});1275 (s) (C−O) ^{1}H− NMR [400 MHz, $CDCl_3$, 300 K] δ/ppm = 0.858 [3× 1 H (CH_3)]; 1.219 [m, 30H (alkyl chain CH_2)]; 1.64 [t, 2 H (−NCH_2CH_2−)]; 2.63 [m 2H (−NCH_2−)]; 3.90 [4H(−NCH_2Py and −NCH_2Ph−]; 7.20 [s, 1H (aryl)]; 7.30 [s, 1H (aryl)] 7.20−7.90 [m, 3H (py)]; 8.61 [d, 1H (py)] ESI pos. in MeOH: m/z = 719.0 for $[HL^{I-ODA} + H^+]^+$.

Synthesis of the Ligand 2,4-Diiodo-6-(((4-(nonyloxy)benzyl)-(pyridin-2-ylmethyl)amino)methyl)phenol, HL^{I-NOBA}. 2-aminomethylpyridine (1.08 g; 10 mmol) was added to the solution of 4-(nonyloxy)benzaldehyde (2.48 g, 10 mmol) in methanol at 50 °C. The yellow solution obtained was stirred for 1 h and then reduced with $NaBH_4$ (0.55 g, 15 mmol) at 0 °C. After 2 h under stirring at room temperature, the solvent was removed and the crude product was added to a 100 mL of 5% aqueous $NaHCO_3$ and extracted with dichloromethane. The combined extracts were dried over $MgSO_4$, and the oil-like product was isolated and vacuum-dried. To a 50 mL dichloromethane solution containing 1.02 g (3 mmol) of the amine and 0.8 mL (6 mmol) of Et_3N was added 1.18 g (3 mmol) of 2,4-di-iodo-6-(chloromethyl)phenol, and the solution was refluxed for 24 h. Upon completion, the product was washed with 5% $NaHCO_3$, and the organic layer was dried in $MgSO_4$, giving an oily product, which was vacuum-dried and characterized by IR, NMR, and Mass analysis. IR (KBr, cm^{-1}) 2855(s), 2933(s) (alkyl- CH-); 1611(m), 1511(m), 1443(s) (C═Npy, C═Car); 1289(s) (C−O) ^{1}H NMR [400 MHz, $CDCl_3$, 300 K] δ/ppm = 0.87 [3 × 1H (CH_3)]; 1.27−1.42 [m, 12H (alkyl chain CH_2)]; 1.75 [m, 2H (−PhO−CH_2CH_2−)]; 3.62 [s 2H (−OPhCH_2N−)]; 3.71 [s, 2H (−NCH_2Ph−]; 3.787[s, 2H (−NCH_2Py−]; 3.91 [t, 2H (−PhOCH2−]; 6.83−7.18 [m, 4H (Ph)]; 7.20−7.90 [m, 3H (py)]; 8.61 [d, 1H (py)] ESI pos. in MeOH: m/z = 699.41 for $[HL^{I-NOBA} + H^+]^+$.

Synthesis of the Complexes. The archetypical complexes **1** and **2** and the metallosurfactants **3** and **4** were synthesized under aerobic conditions using the general procedure described below:

(19) (a) Becke, A. D. *Phys. Rev. A* **1988**, *38*, 3098. (b) Becke, A. D. *J. Chem. Phys.* **1993**, *98*, 5648. (c) Lee, T.; Yang, W. T.; Parr, R. G. *Phys. Rev. B* **1988**, *37*, 785. (d) Ditchfield, R.; Hehre, W. R.; Pople, J. A. *J. Chem. Phys.* **1971**, *54*, 724. (e) Gordon, M. S. *Chem. Phys. Lett.* **1980**, *76*, 163. (f) Hariharan, P. C.; Pople, J. A. *Theor. Chim. Acta.* **1973**, *28*, 213. (g) Hariharan, P. C.; Pople, J. A. *Mol. Phys.* **1974**, *27*, 209. (h) Hehre, W. R.; Ditchfield, R.; Pople, J. A. *J. Chem. Phys.* **1972**, *56*, 225.

(20) Frisch, M. J.; Trucks, G. W.; Schlegel, H. B.; Scuseria, G. E.; Robb, M. A.; Cheeseman, J. R.; Montgomery, J. A., Jr.; Vreven, T.; Kudin, K. N.; Burant, J. C.; Millam, J. M.; Iyengar, S. S.; Tomasi, J.; Barone, V.; Mennucci, B.; Cossi, M.; Scalmani, G.; Rega, N.; Petersson, G. A.; Nakatsuji, H.; Hada, M.; Ehara, M.; Toyota, K.; Fukuda, R.; Hasegawa, J.; Ishida, M.; Nakajima, T.; Honda, Y.; Kitao, O.; Nakai, H.; Klene, M.; Li, X.; Knox, J. E.; Hratchian, H. P.; Cross, J. B.; Bakken, V.; Adamo, C.; Jaramillo, J.; Gomperts, R.; Stratmann, R. E.; Yazyev, O.; Austin, A. J.; Cammi, R.; Pomelli, C.; Ochterski, J. W.; Ayala, P. Y.; Morokuma, K.; Voth, G. A.; Salvador, P.; Dannenberg, J. J.; Zakrzewski, V. G.; Dapprich, S.; Daniels, A. D.; Strain, M. C.; Farkas, O.; Malick, D. K.; Rabuck, A. D.; Raghavachari, K.; Foresman, J. B.; Ortiz, J. V.; Cui, Q.; Baboul, A. G.; Clifford, S.; Cioslowski, J.; Stefanov, B. B.; Liu, G.; Liashenko, A.; Piskorz, P.; Komaromi, I.; Martin, R. L.; Fox, D. J.; Keith, T.; Al-Laham, M. A.; Peng, C. Y.; Nanayakkara, A.; Challacombe, M.; Gill, P. M. W.; Johnson, B.; Chen, W.; Wong, M. W.; Gonzalez, C.; Pople, J. A. *Gaussian 03*, revision C.02; Gaussian, Inc.: Wallingford, CT, 2004.

(21) Schlegel, H. B. *J. Comp. Chem.* **1982**, *03*, 214.

(22) Shakya, R.; Peng, F.; Liu, J.; Heeg, M. J.; Verani, C. N. *Inorg. Chem.* **2006**, *45*, 6263.

Scheme 2

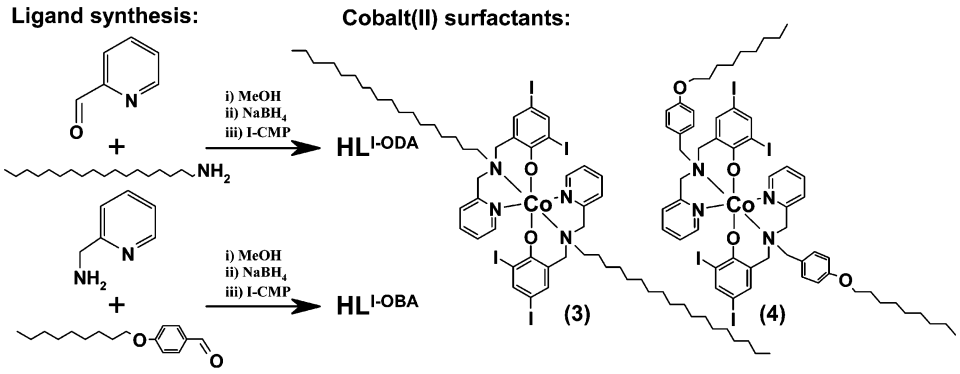

A solid sample of $[Co(H_2O)_6](ClO_4)_2$ (0.37 g, 1.0 mmol) was added to a 30 mL MeOH solution containing 2.0 mmol of the appropriate ligand and Et_3N (0.28 mL; 2.0 mmol). The solution was stirred at room temperature for 1 h. A yellowish-brown muddy product was vacuum filtered and washed with cold methanol and ether. The product was recrystallized using a 1:1 solvent mixture of methanol and dichloromethane.

$[Co^{II}(L^{IA})_2]\cdot 2CH_3OH$ (1). Yield = 81% Anal. Calcd for $C_{28}H_{30}N_4Co_1I_4O_4$: C, 31.93; H, 2.87; N, 5.32. Found: C, 32.81, H, 2.63, N 5.32. IR (KBr, cm^{-1}) 1603(m), 1561(s), 1448(s) (C═Npy, C═CAr); 1328(m) (C−O); ESI Pos. in MeOH: *m*/*z* (100%) = 989.6 for $[Co^{II}(L^{IA})_2 + H^+]^+$.

$[Co^{II}(L^{BrA})_2]\cdot CH_3OH$ (2). Yield = 79% Anal. Calcd for $C_{27}H_{26}N_4Co_1Br_4O_3$: C, 38.93, H, 3.15, N 6.73. Found: C, 39.43, H, 3.09, N 6.65. IR (KBr, cm^{-1}) 1603(m), 1572(s), 1454(s) (C═Npy, C═CAr); 1328(m) (C−O); ESI Pos. in MeOH: *m*/*z* (100%) = 798.8 for $[Co^{II}(L^{BrA})_2+H^+]^+$.

$[Co^{II}(L^{I-ODA})_2]$. (3). Yield = 76% Anal. Calcd for $C_{62}H_{94}N_4Co_1I_4O_2$: C, 49.84, H, 6.34, N 3.75. Found: C, 49.79, H, 6.29, N 3.67. IR (KBr, cm^{-1}) 2852(s), 2923(s) (alkyl− CH−); 1605(m), 1562(s), 1447(s) (C═Npy, C═CAr); 1329(m) (C−O); ESI Pos. in MeOH: *m*/*z* (100%) = 1493.8 for $[Co^{II}(L^{I-ODA})_2+H^+]^+$.

$[Co^{II}(L^{I-NOBA})_2]\cdot CH_2Cl_2$ (4). Yield = 79% Anal. Calcd for $C_{59}H_{72}N_4Co_1I_4Cl_2O_4$: C, 46.05; H, 4.72; N, 3.64. Found: C, 45.89, H, 4.74, N 3.67. IR (KBr, cm^{-1}) 2853(s), 2922(s) (alkyl− CH−); 1607(m), 1561(s), 1446(s) (C═Npy, C═CAr); 1326(m) (C−O); ESI Pos. in MeOH: *m*/*z* (100%) = 1454.7 for $[Co^{II}(L^{I-NOBA})_2+H^+]^+$.

Results and Discussion

Synthesis and Characterization of the Archetypes 1 and 2. The archetypical ligands HL^{BrA} and HL^{IA} were synthesized as reported in our previous work.[15,23] Aiming at the synthesis of cobalt(III) complexes with the bromo- and iodo-substituted ligands HL^{BrA} and HL^{IA} under aerobic conditions, a pale-yellowish-brown precipitate formed immediately after the addition of $[Co^{II}(H_2O)_6](ClO_4)_2$ in methanol. After stirring the mixture at room temperature for 1 h, the precipitate was frit-filtered, vacuum-dried, and characterized by IR spectroscopy, ESI spectrometry, and elemental analysis. The IR spectra of **1** and **2** show the usual bands expected for the ligands with minor shifting indicative of metal coordination but lack the expected peaks for the perchlorate counterion at ca. 1097 cm^{-1}. The ESI mass analysis evidence $[M+H]^+$ peak clusters for **1** and **2** with the proper mass and isotopic distribution. Because the ^{59}Co ion presents 100% abundance, the isotopic distribution is attributed to the presence of carbon, nitrogen, and oxygen atoms. Elemental analysis also provided compelling evidence for **1** and **2** to contain bivalent cobalt ions. The UV−visible spectra of **1** and **2** differ significantly from those of trivalent cobalt in similar environments[15] in which the characteristic phenolate-to-cobalt(III) charge transfer is missing. Final evidence about the oxidation state of the metal center came via the X-ray diffraction analysis of the iodo-substituted **1**, in which the absence of counterions is confirmed. EPR spectroscopy, expected to be silent in low-spin $3d^6$ cobalt(III) species, also yielded a signal for cobalt(II). The stabilization of these cobalt(II) complexes is related, at least partially, to the low solubility of the complexes in methanol. A full discussion of this data is offered later in this article.

Synthesis and Characterization of the Metallosurfactants 3 and 4. To explore the stabilization of bivalent cobalt and to aim at the development of amphiphilic materials based on these archetypes, we synthesized the new ligands HL^{I-ODA} and HL^{I-NOBA}. The ligands incorporate, respectively, amphiphilic octadecyl and nonyloxybenzyl moieties attached to the secondary amine of HL^{IA}. Initial attempts to synthesize HL^{I-ODA} and HL^{I-NOBA} using picolyl chloride, as described in similar procedures,[24] yielded less-than-satisfactory results. In an attempt to improve the ligand synthesis, the new precursor I−CMP (2,4-di-iodo-6-(chloromethyl)phenol) was obtained. Treatment of 2-hydroxy-3,5-diiodobenzaldehyde with $NaBH_4$ gave the corresponding alcohol that was treated with thionyl chloride, yielding the desired precursor. The new ligands HL^{I-ODA} and HL^{I-NOBA} were synthesized by the treatment of the appropriate aldehyde with the amine counterpart, followed by the reduction and nucleophillic substitution with I−CMP, as shown in the left-hand side of Scheme 2. The ligands were thoroughly characterized by NMR, IR spectroscopy, and ESI mass spectrometry. The cobalt-containing surfactants **3** and **4** are shown in the right-hand side of Scheme 2 and were synthesized by reacting a methanol solution of the corresponding ligand with $[Co^{II}(H_2O)_6](ClO_4)_2$ in a 2:1 ligand-to-metal molar ratio at 40 °C for 1 h. In both cases, a yellowish muddy precipitate was

(23) Imbert, C.; Hratchian, H. P.; Lanznaster, M.; Heeg, M. J.; Hryhorczuk, L. M.; McGarvey, B. R.; Schlegel, H. B.; Verani, C. N. *Inorg. Chem.* **2005**, *44*, 7414−7422.

(24) Neves, A.; Romanowski, S. M.; Vencato, I.; Mangrich, A. S. *J. Chem. Soc., Dalton Trans.* **1998**, 617.

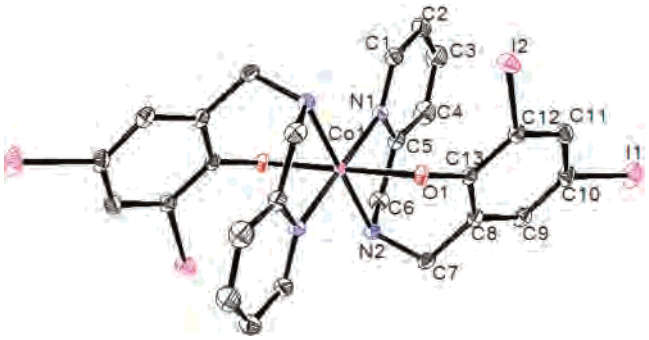

Figure 1. ORTEP representation at 50% probability for **1**. Hydrogen atoms excluded for clarity. Selected bond lengths (Å): Co1−O1 = 2.0746(11), Co1−N2 = 2.1558(14), Co1−N1 = 2.1220(14), C13−O1 = 1.3156(19), C7−C8 = 1.500(2), C7−N2 = 1.490(2), N2−C6 = 1.473(2), C5−C6 = 1.508(3). Bite angles (°): O1−Co1−N2 = 89.48(5), N1−Co1−N2 = 79.59-(5). Average distances (Å): C−C in Py = 1.383(3), C−N in Py = 1.340-(2), C−C in Ph = 1.400(2), C−I = 2.0992(16)

Table 1

formula	$C_{28}H_{30}N_4O_4I_4Co$
fw	1053.09
space group	*P*2(1)/*c*
a (Å)	12.5495(5)
b (Å)	11.1716(4)
c (Å)	12.3229(4)
β (deg)	97.435(1)
V (Å^3)	1713.1(1)
Z	2
T (K)	100(2)
λ (Å)	0.71073
density$_{calcd}$ (g cm^{-3})	2.042
μ (mm^{-1})	4.142
R(F)[a] (%)	2.03
Rw(F) (%)	4.66

[a] $R(F) = \sum||F_o| - |F_c||/\sum|F_o|$; $Rw(F) = [\sum w(F_o^2 - F_c^2)^2/\sum w(F_o^2)^2]^{1/2}$ for $I > 2\theta(I)$.

isolated by frit filtration, washed with excess cold methanol, and vacuum-dried for several days, yielding amorphous powders after recrystallization in methanol/dichloromethane. The IR features for **3** and **4** resemble those in the corresponding ligands, with minor shifts indicative of metal coordination and absent perchlorate peaks. The ESI mass analyses of the complexes show masses and isotopic distributions in good agreement with the $[M+H^+]^+$ ion. Similar to archetypes **1** and **2**, the UV−visible spectra show the absence of the ligand-to-metal charge-transfer band that is characteristic of cobalt(III) complexes that contain phenolates.

Molecular Structure of Archetype 1. The molecular structure of **1** was determined by X-ray crystallography with single crystals obtained from slow evaporation of a 1:1 solvent mixture of methanol and dichloromethane. The ORTEP diagram for **1** is depicted in Figure 1 with selected bond lengths and angles provided in Table 2. Analogous to the previously reported cobalt(III) complexes,[15] the structure of this complex is composed of a pseudo-octahedral metal center surrounded by two tridentate $(L^{IA})^-$ ligands adopting a sym-fac coordination.[25] The cobalt ions are in a centrosymmetric environment described in a Bailar, Miessler, and Tarr notation[26] as $[Co\langle N_{am1}N_{am2}\rangle\langle N_{py1}N_{py2}\rangle\langle O_{phen1}O_{phen2}\rangle]$, meaning that the equivalent donor sets in both ligands are trans to each other. The cobalt(II) center adopts an approximate D_{2h} symmetry, with its nearest neighbors and a $Co^{II}-O_{phenolate}$ distance of 2.07 Å that is comparable to others found in the literature;[27] however, being longer than those for the previously reported $Co^{III}-O_{phenolate}$.[15] Although some caution is necessary with pseudo-octahedral systems, the increment in the bond length can be explained as a consequence of Jahn−Teller distortion in a high-spin cobalt(II) $3d^7$ system with $S = {}^3/_2$. The average $Co-N_{amine}$ (2.16 Å) and the average $Co-N_{pyridyl}$ bond length (2.12 Å) are also in good agreement with previously reported values,[13b,28] and are similarly longer that the equivalent value of 1.95−1.96 Å in trivalent complexes. Assuming this "trans-phenolates" geometry as the preferential one, as will be shown by the DFT calculations, a correlation between the structure of archetype **1** and amphiphiles **3** and **4** can be drawn.

Table 2. Comparison of Molecular Orbital Energies and Compositions for $[Co(L^A)_2]^+$ with Trans-Phenolates and Cis-Phenolates Configurations[a]

	Energy		Symmetry		% Metal		% Ligand	
	trans	cis	trans	cis	trans	cis	trans	cis
LUMO+1	−0.98	−0.93			0.9	1.0	99.1	99.0
LUMO	−1.06	−0.95			0.6	2.8	99.4	97.2
HOMO	−4.11	−4.25	a_g		19.7	9.1	80.3	90.9
HOMO −1	−4.52	−4.41	b_{2u}		1.1	10.3	98.9	89.7
HOMO −2	−4.82	−5.14	b_{1g}		21.4	28.4	78.6	71.6
HOMO −3	−5.39	−5.42	a_g		47.7	19.8	52.3	80.2
HOMO −4	−5.85	−5.82			0.3	25.2	99.7	74.8
HOMO −5	−5.85	−5.85			0.1	0.0	99.9	100.0
HOMO −6	−5.99	−5.88	b_{2u}		3.6	9.2	96.4	90.8
HOMO-7	−6.26	−6.37	b_{3g}		74.0	25.5	26.0	74.5

[a] The trans-phenolates configuration for $[Co(L^A)_2]^+$ is described by $[Co\langle N_{am1}N_{am2}\rangle\langle N_{py1}N_{py2}\rangle\langle O_{phen1}O_{phen2}\rangle]$, whereas the cis-phenolates configuration is $[Co\langle N_{am1}O_{phen2}\rangle\langle O_{phen1}N_{am2}\rangle\langle N_{py1}N_{py2}\rangle]$. The $N_{py1}-Co-N_{py2}$ axis has been placed along the *z* direction; the *y* axis bisects the $O_{phen1}-Co-O_{phen2}$ angle; the *x* axis bisects the $N_{am1}-Co-N_{am2}$ angle. Energy is given in eV. Pseudo symmetry labels have been assigned according to the D_{2h} group. For nonbonding orbitals, pseudo-symmetry labels are given only where ligand orbitals mimic symmetry-adapted linear combinations. % Metal and % Ligand correspond to the character of the molecular orbitals.

EPR Spectroscopy of Archetypes 1 and 2. The EPR spectra of **1** and **2** have been measured to assess the oxidation state, geometry, and electronic configuration of the archetypes. In a pseudo-octahedral D_{2h} symmetry, the $d_{x^2-y^2}$ and d_{z^2} orbitals transform as a_g, whereas d_{xy}, d_{xz}, and d_{yz} transform respectively as b_{1g}, b_{2g}, and b_{3g}. The b_{xg} set has closely related energies and is separated from the a_g set by a large energy gap. A low-spin electronic configuration given by

(25) Kepert, D. L. *Inorganic Stereochemistry*, Springer-Verlag: New York 1982, p 114.

(26) The notation $\langle A_1B_2\rangle$ indicates that A is trans to B, with A and B corresponding to the pyridine (Npy), amine (Nam), or phenolato (Ophen) groups. Subscripts 1 and 2 designate respectively the first and the second ligand. This concise notation saves space and was adapted by G. Miessler and D. Tarr in *Inorganic Chemistry*, Pearson-Prentice Hall, 2004, pp 311−315, from the original work by John Bailar, Jr., in *J. Chem. Ed.* 1957, **34**, 334 and 623. The link to Prof. Bailar's work has been explained by Prof. Miessler in a personal communication.

(27) Higgs, T. C.; Carrano, C. J. *Inorg. Chem.* **1997**, *36*, 291.

(28) (a) Mohamadou, A.; Jubert, C.; Barbier, J. *Inorg. Chim. Acta* **2006**, *359*, 273, (b) Comba, P.; Kerscher, M.; Merz, M.; Müller, V.; Pritzkow, H.; Remenyi, R.; Schiek, W.; Xiong, Y. *Chem.—Eur. J.* **2002**, *8*, 5750, (c) Makowska-Grzyska, M. M.; Szajna, E.; Shipley, C.; Arif, A. M.; Mitchell, M. H.; Halfen, J. A.; Berreau, L. M. *Inorg. Chem.* **2003**, *42*, 7472.

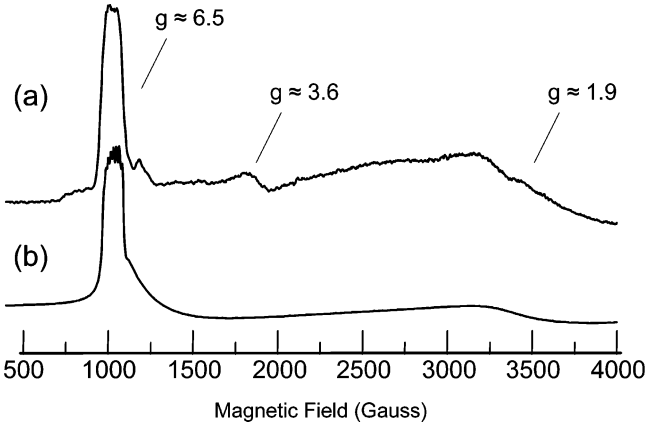

Figure 2. (a) Frozen liquid spectrum of **1** in methanol/dichloromethane at 4.1 K. (b) Simulation of the spectra observed for **1** and **2**.

$[a_g^0,a_g^0,b_{1g}^2,b_{2g}^2,b_{3g}^2]$ is expected for a cobalt(III) ion and is thus associated with a lack of signal typical of diamagnetic species. Therefore, the fact that we can observe a signal at ca. 4 K per se is indicative of the presence of cobalt(II) ions. This is in excellent agreement with the lack of a counterion observed independently by IR spectroscopy and X-ray crystallography. The spin Hamiltonian that represents transitions in the lowest Kramer's doublet for $S = {}^3/_2$ in a near-octahedral $3d^7$ configuration is given by $H = \beta_e[g_xH_xS_x+g_yH_yS_y+g_zH_zS_z] + A_xS_xI_x + A_yS_yI_y + A_zS_zI_z$,[29] where S is taken to be $S = {}^1/_2$. EPR measurements are only possible at liquid helium temperatures for cobalt (II) as a result of short spin−lattice relaxation times. The spectra become broader as the temperature is increased, and at liquid nitrogen temperatures (∼77 K) the signal disappears.

Both **1** and **2** exhibit essentially identical features with distinct signal-to-noise ratios. The frozen-liquid spectrum of **1** in methanol/dichloromethane at 4.1 K is shown in part a of Figure 2 as the first derivative of the absorption spectrum. The most-prominent feature in the spectra is a peaklike signal at ca. 1000 G, which is a turning point for a broad line with a principal g value of 6.5 and two other signals with much-smaller g values. The narrow shape of the peak is due to a small hyperfine interaction for the isotope ^{59}Co ($I = {}^7/_2$) for this principal direction (attributed to z). To illustrate the origin of this peak, we show in part b of Figure 2 a simulation for $g_z = 6.5$ and $A_z = 16$ G, with the other principal directions having identical values of $g_{x,y} = 1.9$ and $A_{x,y} = 100$ G. At the base of the $g = 6.5$ peak, there appears to be another peaklike feature with $g = 6.9$ and a resolved hyperfine interaction of about 60 G. A turning point is also seen at $g = 3.58$, and another intense broad turning point is seen at $g = \sim 1.9$. It suggests that two different cobalt(II) species are present in solution, and because of the labile nature of the ion, these are most likely different conformers formed in solution. Similar behavior has been reported for other divalent cobalt species.[30,31]

In near-octahedral fields, the orbital motion in the $^4T_1$ ground state of cobalt(II) is not quenched, resulting in a large spin−orbit interaction, which produces a Kramer's doublet ground state. This Kramer's doublet is always fitted to an $S = {}^1/_2$ spin Hamiltonian. The EPR signal of a high-spin cobalt(II) ion in a nondistorted-octahedral environment exhibits a single $g \approx 4.34$. If distortion of this octahedral field occurs, three different g values ranging from 6.9 to 2.0 are observed. In tetrahedral and cubic fields, the g value is near 2.3. For low-spin cobalt(II) ions resulting from strong crystal fields with large distortions, g values will be slightly different than 2.0. On the basis of this discussion, the EPR results indicate **1** and **2** as being high-spin in nature and located in a pseudo-octahedral environment.

Electronic Structure Calculations. In a recent article, we investigated iron(III) and gallium(III) complexes of asymmetric NN′O ligands,[23] concluding that facial coordination of the ligands is favored, along with a cis distribution of the phenolates. In an account on trivalent cobalt complexes,[15] we have shown that phenolate rings adopt a trans configuration in a D_{2h} local symmetry, favored by at least 4.0 kcal/mol. Here, we are interested in assessing the D_{2h} facial, all-trans geometry observed experimentally for **1**, to infer whether it is reasonable to expect **3** and **4** to have a similar local D_{2h} trans ligand configuration. A comparison between bivalent and trivalent cobalt is also included. The same level of theory was employed throughout the calculations in this and in the aforementioned accounts, thus allowing direct comparisons.

Complex **1** has a $3d^7{}_{\text{high spin}}$ cobalt(II) center and iodo substituents in the second and fourth positions of the phenolate moiety of the ligand. To make the calculations more affordable, these groups are replaced by hydrogen atoms, and the resulting model is called $\mathbf{1^H}$. Considering this a suitable model, the energetics of the cobalt(II) complexes with cis and trans phenolates, described respectively as $[\langle N_{am1}N_{am2}\rangle\langle N_{py1}O_{phen2}\rangle\langle O_{phen1}N_{py2}\rangle]$ and $[\langle N_{am1}N_{am2}\rangle\langle N_{py1}N_{py2}\rangle\langle O_{phen1}O_{phen2}\rangle]$, were compared. The optimized geometry of the trans isomer of $\mathbf{1^H}$ is in good agreement with the crystal structure of **1** and is depicted in the top left-hand side of Figure 3.

The calculations favor the trans configuration of $\mathbf{1^H}$ by 2.3 kcal·mol^{-1}. This energy difference between isomers is similar to the 3.8 kcal·mol^{-1} isomer difference observed for the equivalent cobalt(III) model complexes.[15] Despite the small energy difference, our computational results do agree with the experimentally observed preference for the trans isomer. Similar to the cobalt(II) case,[15] the energy preference can be understood by considering the energies of the frontier molecular orbitals (Table 2). The MOs of $\mathbf{1^H}$ reveal some metal character in the HOMO, HOMO-2, and HOMO-3 orbitals for the trans structure, as shown in the right-hand side of Figure 3 and in Table 2, indicating that these are the d-based orbitals in a pseudo-octahedral D_{2h} symmetry related to the high-spin electronic configuration $[a_g^1,b_{1g}^1,a_g^1,b_{3g}^2,b_{2g}^2]$

(29) McGarvey, B. R. *Transition Metal Chemistry*; Carlin, R. L., Ed.; Marcel Dekker, Inc.: New York, 1966, vol. 03, p 175.
(30) Scarpellini, M.; Wu, A. J.; Kampf, J. W.; Pecoraro, V. L. *Inorg Chem.* **2005**, *44*, 5001.
(31) Tubbs, K. J.; Szajna, E.; Bennett, B.; Halfen, J. A.; Watkins, R. W.; Arif, A. M.; Berreau, L. M. *Dalton* **2004**, 2398.

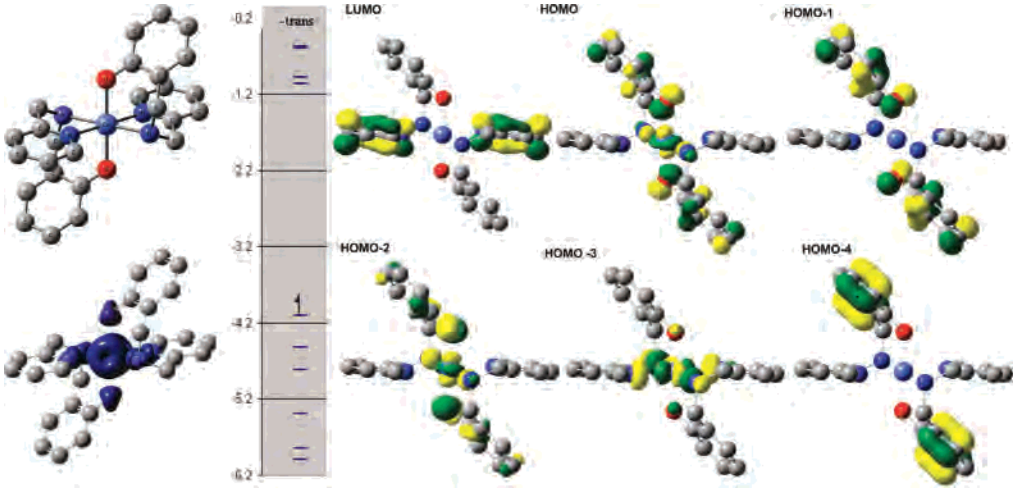

Figure 3. Left: Minimized structure exhibiting the favored trans-phenolates configuration for $\mathbf{1^H}$ (top) and the equivalent spin-density plot (bottom). Center: Orbital energy ladder for the model $\mathbf{1^H}$. Right: Selected frontier MOs for the trans $\mathbf{1^H}$ showing prevalent metal or ligand character.

with an $S = {}^3/_2$ ground state. These correspond to the singly occupied orbitals, and the $b_{1g}{}^1$ MO lies slightly higher in energy than the $a_g{}^1$ orbital. Both HOMO and HOMO-2 orbitals show considerable phenolate character via the contribution of the 2p orbitals in the oxygen centers, whereas the HOMO-3 orbital entails sigma interactions within the *xz* plane, thus consistent with the four nitrogen donors combining with a $d_{z^2-x^2}$ orbital. This $d_{z^2-x^2}$ component is part of the linear combination for the d_{z^2} orbital, more appropriately described as $d2_{z^2-x^2-y^2}$ (combination of $d_{z^2-x^2}$ and $d_{z^2-y^2}$), thus transforming as a_g in a D_{2h} group. These results are consistent with our expectations described in the EPR section above. Whereas the highest-occupied MOs displaying metal character have similar energies for both the cis and trans isomers, the second-highest-occupied MO for the trans structure is 0.4 eV more stable than the corresponding cis MO. This trend continues to the third- and fourth-highest-occupied MOs, with the trans isomer MOs being more stable by 0.3 and 0.8 eV. We also note that the relative stability of the trans isomer, relative to the cis geometry, may increase if we had not replaced the iodo groups in **1** with hydrogen atoms. Indeed, preliminary results from a study in our labs related to similar complexes suggest that replacement of the hydrogen atoms by chlorides in the phenolate moiety leads to an increase in the stabilization of the favored isomer by ca. 7.0 kcal·mol^{-1}.[32] Although the presence of different conformers cannot be ruled out, as discussed in the EPR section, it seems reasonable from these results to predict that the prevalent trans geometry is also found in the metallosurfactants **3** and **4**.

Figure 3 also shows the spin-density plot for $\mathbf{1^H}$, and it is clear that the majority of the excess spin density is localized on the metal center, with a small degree of excess spin on the immediate six neighbors of the coordination sphere. Specifically, the cobalt center has a net Mulliken spin population of 2.74, consistent with an oxidation state assignment of a bivalent cobalt ion.

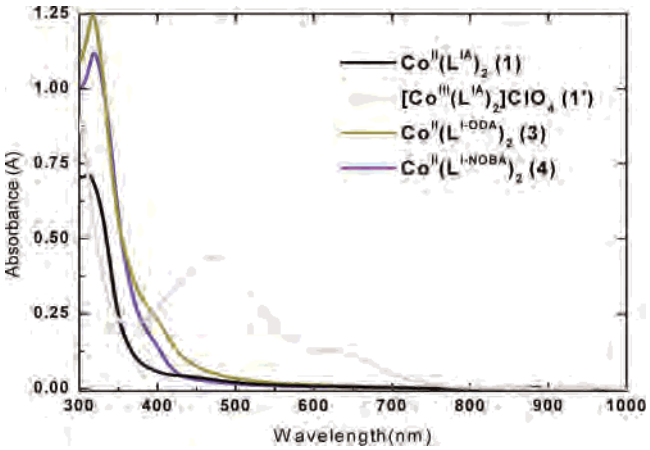

Figure 4. UV−vis spectra of 1.0×10^{-4} M dichloromethane solutions for **1**, **1′**, **3**, and **4** at room temperature. Assignments λ (nm)/ϵ (Lmol^{-1}cm^{-1}) are as follows: For **1** (black trace): 264/21085; 312/7122. For **2** (not shown): 262/24 777; 316/8814. For **3** (dark-yellow trace): 257/31 981; 317/12 324. For **4** (purple trace): 264/31 981; 321/11 149. For **1′**: 282/10 202; 474/4389; 631/1320.

Electronic Spectroscopy of 1−4. The UV−vis spectra of **1**−**4** were taken in 1.0×10^{-4} M dichloromethane solutions. The spectra of selected complexes are shown in Figure 4. The main feature observed for **1**−**4** is the presence of intense $\pi \rightarrow \pi^*$ intraligand bands between 312 and 321 nm. The most-remarkable indication of the bivalent nature of these species is the lack of the $p\pi_{phenolate} \rightarrow d\sigma^*_{cobalt(III)}$ charge-transfer band found at 474 nm for the iodo-substituted cobalt(III) **1′** and is systematically found between 430 and 470 nm for the previously reported cobalt(III) complexes with similar ligands.[15] This observation is in agreement with the expected spectrum of d^7 high-spin cobalt(II) systems.[33] The absence of the LMCT band for the bivalent species when compared to equivalent trivalent species is reflected by a considerable decrease in the color of the complexes and suggests that optical responsiveness can be attained either by means of electrochemical or chemical stimuli.

(32) Allard, M.; Verani, C. N., unpublished results. These results are part of an upcoming article on the chemistry of iron-containing amphiphiles.

(33) Lever, A. B. P. *Inorganic Electronic Spectroscopy*; Elsevier Science: New York, 1984; pp 203−245.

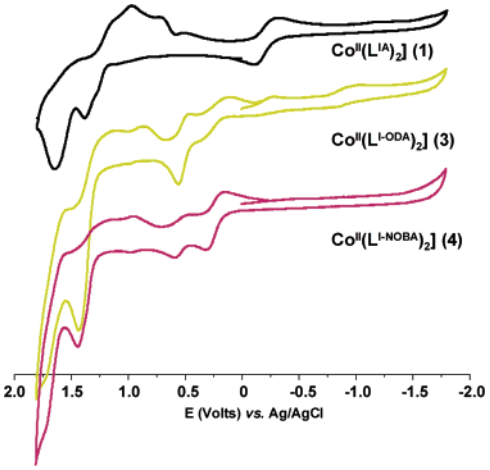

Figure 5. CVs of **1** (black trace), **3** (dark-yellow trace), and **4** (violet trace) as 1.0×10^{-4} M dichloromethane solutions with 0.1 mol L^{-1} $TBAPF_6$ at room temperature. Scan rate at 100 mV·s^{-1} using a three-electrode system (W = carbon, ref = Ag/AgCl, Aux. = platinum wire). Ferrocene was used as an internal standard ($E_{1/2}$ = 0.40 V).

Redox Properties of 1−4. Cyclic voltammograms of **1**−**4** were measured in dichloromethane using $TBAPF_6$ as a supporting electrolyte to evaluate the response of the compounds toward redox stimuli in the time scale of the voltammetric experiments. The cyclic voltammograms of **1**, **3**, and **4** are shown in Figure 5, and the potentials are given in Table 3. Unexpectedly, an intricate redox behavior is observed for each of these complexes, much different from that observed for the equivalent cobalt(III) chloro-substituted analogue [$Co^{III}(L^{Cl2A})_2$] published previously.[15] Analogue [$Co^{III}(L^{Cl2A})_2$] has shown a reversible behavior with potentials for the cobalt(III)/cobalt(II) couple observed at −0.67 versus Fc^+/Fc, whereas quasi-reversible ligand-centered processes were observed at 0.87 and 1.29 versus Fc^+/Fc. It is evident from the shape of the voltammograms for **1**, **3**, and **4**, as well as by the amplitude of the different processes, that multiple reductions and oxidations take place at the surface of the electrode. The behavior of **1** resembles accurately that for **2** (not shown).

Ligand-centered oxidations around 1.5 and 1.75 V (vs Ag/AgCl) can be observed in all of the species, falling within the expected range observed for the chloro-substituted analogue and related to the oxidation of phenolates to phenoxyl radicals. Nonetheless, each of these processes give rise to multiple ligand-based reductions tentatively attributed to the phenoxyl-to-phenolate process in the species derived from the parent complexes. Three reductions for **1** and **2** and two for **3** and **4** are observed even when cycling of the potential happens immediately after the formation of the first phenoxyl radical. It suggests that a single oxidation suffices to trigger follow-up reactions, probably polymeric in nature and associated to the activation of the iodo groups. The metal-centered processes in **1** and **2** are found to be quasi-reversible and within comparable potentials to that of the chloro analogue [$Co^{III}(L^{Cl2A})_2$]. The scenario changes considerably for **3** and **4**, where once again multiple processes indicative of catalytic decomposition take place. This behavior is consistent within several scan rates at 50, 100, and 500 mV·sec^{-1} in dichloromethane. Finally, the use of successive scanning (∼15 cycles) in dichloromethane at 100 mV·sec^{-1} reveals film formation at the surface of the electrode, as characterized by an increase of the peak current after each scan.[9] One can conclude that the replacement of either *tert*-butyl or chloro groups by iodo substitutents in the phenol ring fails in leading to improved redox responses based on metal or ligand activities. Although this fact limits the use of these amphiphiles as responsive materials considerably, the presence of iodo-substituted phenols might be key in the development of conductive polymerized films and will be further explored in our lab.

Amphiphilic Properties, Brewster Angle Microscopy, and Langmuir Film Formation of HL^{I-ODA}, HL^{I-NOBA}, 3, and 4. The logic behind the synthesis of the ligands HL^{I-ODA} and HL^{I-NOBA} consists of attaching simple organic fragments of nonpolar nature to the amine nitrogen of the archetypical **1**. These organic fragments are expected to confer amphiphilic properties to the newly synthesized systems in which the octadecyl and nonyl-oxo-benzene fragments, respectively present in HL^{I-ODA} and HL^{I-NOBA}, act as hydrophobic counterparts of a polar head group. Inclusion of a metal ion such as cobalt(II) is expected to modify the amphiphilicity of the system as a result of changes in the molecular dipole moment and the coordination to two of the amphiphilinc ligands to one metal center, forming new species. The amphiphilic properties of both ligands, **3** and **4**, are displayed in Figure 6 as compression isotherms plotting surface pressure (Π, mN·m^{-1}) versus area per molecule (A, $Å^2$). These isotherms give information about the 2D behavior of the resulting Langmuir film at the air/water interface, the collapse pressure (π_c), and the area at the collapse of the monolayer (A_c). The surfactant is initially dissolved in an immiscible organic solvent and subsequently spread on the water surface. As the barriers of the trough are compressed, the tension (γ) of the air−water interface in the presence of the amphiphilic species decreases as compared to that of the bare air−water interface (γ_0 = 72 mN·m^{-1} at 23 °C), resulting in an increase in Π ($= \gamma_0 - \gamma$). The isotherms for HL^{I-ODA}, HL^{I-NOBA}, **3**, and **4** reveal that all of the species are interfacially active. Each isotherm was repeated at least three times, and excellent reproducibility was attained.

The individual molecules of the protonated ligands start interacting with each other at the air/water interface at ca. 45 $Å^2$·$molecule^{-1}$ for both ligands, forming an expanded phase.[34] No phase transitions were observed, and collapse pressures of ca. 20 mN·m^{-1} were recorded. Areas at collapse of 41 and 35 $Å^2$·$molecule^{-1}$ for HL^{I-ODA} and HL^{I-NOBA} respectively can be determined by extrapolating the Π versus A curve at its steepest slope before the collapse, where it intercepts the *x* axis.[1] The A_c values determined for the

(34) For monolayers, it is common to use the terms gaseous (G), expanded (E), and condensed (C) to describe the phases. In G-phases, the molecules of the monolayer are far apart from each other so that minimal force is exerted on one another. In E-phases, interactions among the molecules are semi-randomic, resembling interactions in a liquid. C-phases resemble interactions in a solid. For an excellent introductory text on the subject, see Petty, M. C. "Langmuir−Blodgett Films".

Table 3

compounds	reductions[a] (V vs F_c^+/F_c)	oxidations[b] (V vs F_c^+/F_c)
(**1**)	−0.74, +1.01, +0.67, +0.50, +0.23	−0.58, +0.79, +0.91, +1.17
(**2**)	−0.81, +1.15, +0.71, +0.55, +0.27	−0.68, +0.80, +0.89, +1.17
(**3**)	−0.72, +1.10, +0.74, +0.66, +0.41, +0.02, −0.32	−0.60, −0.11, +0.11, +0.98, +1.27
(**4**)	−0.25, +1.15, +0.83, +0.74, +0.52, +0.07	−0.11, +0.17, +0.55, +1.02. +1.31

[a] The potential given is the cathodic peak potential E_{pc} versus F_c^+/F_c. [b] The potential given is the anodic peak potential E_{pa} versus F_c^+/F_c.

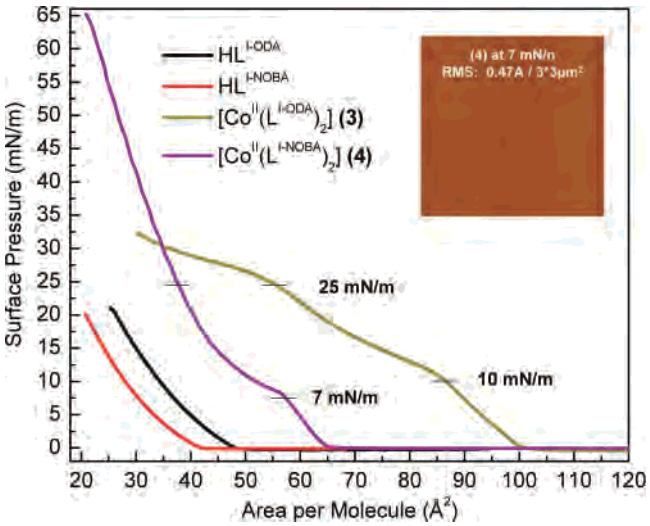

Figure 6. Compression isotherms at the air/water interface for HL^{I-ODA} (black), HL^{I-NOBA} (red), (**3**) (dark yellow), and (**4**) (violet). Inset: Tapping mode AFM (topography) of **4** at 7 mN·m^{-1}. Pressures by which LB films were deposited are indicated at 7, 10, and 25 mN·m^{-1}.

ligands are much larger than the 20−22 Å^2·molecule^{-1} observed for heptadecanoic acid[35] but closer to the area occupied by bulkier species like eruric and dimyristolphosphatidic acid (38 and 51 Å^2·molecule^{-1}).[36]

Drastic changes are observed in the amphiphilic properties when the ligands are compared to the cobalt complexes. The individual molecules of **3** start interacting at the air/water interface at ca. 100 Å^2·molecule^{-1}, whereas the molecules of **4** interact at a much lower area of ca. 65 Å^2·molecule^{-1}. We start the discussion with the isotherm of **4**, which exhibits a phase transition at about 8 mN·m^{-1}, forming a condensed phase that collapses with a sudden drop in pressure after 65 mN·m^{-1} with an average area of 48 Å^2·molecule^{-1}. The collapse shows the signature of a constant-area collapse.[37] An increase of ca. 10−15 Å^2·molecule^{-1} in the A_c value is observed when **4** is compared to HL^{I-NOBA}. Considering some rearrangements of the hydrophobic chains, this increase is in agreement with simple molecular mechanics calculations that suggest **4** to be only ca. 18 Å longer than the nonmetallated ligand. Additionally, it has been observed independently by us[38] and others[39] that an increase of about 10 Å^2·molecule^{-1} can be expected upon complexation of

Scheme 3

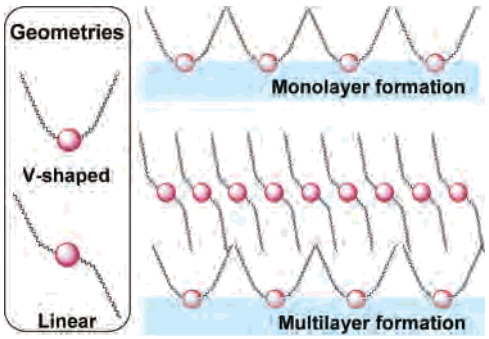

bivalent ions. **3** displays an intricate profile that includes two inflections, at about 13 and 24 mN·m^{-1}, followed by expansions of the areas occupied per molecule. Contrary to the clear collapse observed for **4**, the moving barriers of the trough come to touch each other without a noticeable drop in pressure. This behavior differs from the expected constant-area collapse of a monolayer and led us to consider the isotherm for **3** as representative of the growth of a collapsing monolayer. Understanding that the kinetics of monolayer collapse has been best described as confused,[40] recent work[36,41] may be helpful in this discussion. In monolayers of divalent metal (manganese, cobalt, cadmium, and lead) complexes of stearic acid formed in situ, the nature of the metal ion determines whether collapse happens at constant area or pressure.[42] The formation of a plateau is the signature of a constant-pressure collapse, and all of the monolayers follow the Ries mechanism[43] of folding, bending, and breaking into multilayers. Similar to these metal-containing fatty acids, **3** and **4** exhibit a head group connected to two tail groups, and, therefore, two arrangements are possible: a v-shaped geometry that allows for monolayer formation due to its amphiphilic nature, and a linear geometry (Scheme 3). The latter is unstable at the air/water interface but can form domains or layers on top of hydrophobic interfaces such as the monolayer resulting from the v-shaped geometry.

Hence, we suggest that in the case of **3**, where octadecyl chains are attached directly to the tertiary nitrogen of the head group, unrestricted movement may allow for both the v-shaped and the linear geometries (depicted in Schemes 2 and 3). This leads to constant-pressure collapse followed by the formation of multilayers. On the other hand, the presence of the alkoxy groups in **4** leads to a less-flexible molecule,

(35) Goncalves da Silva, A. M. P. S.; Armitage, D. A.; Linford, R. G. *J. Colloid Interface Sci.* **1993**, *156*, 433.
(36) Petty, M. C. *Langmuir−Blodgett Films*; Cambridge University Press: New York, 1996; pp 65−93.
(37) Kundu, S.; Datta, A.; Hazra, S. *Phys. Rev.* **2006**, *E 73*, 051608
(38) Driscoll, J.; Jayathilake, H.; Wu, L.; Bordenyuk, A.; Heeg, M. J.; Verani, C. N.; Benderskii, A.; da Rocha, S. R. P. submitted to *Langmuir*.
(39) Kraus, S.; Mandler, D. *Langmuir* **2006**, *22*, 7462.
(40) Ybert. C.; Lu, W.; Moeller, G.; Knobler, C. M. *J. Phys.: Condens. Matter* **2002**, *14*, 4753.
(41) Vaknin, D.; Bu, W.; Satija, S. K.; Travesset, A. *Langmuir* **2007**, *23*, 1888.
(42) Kundu, S.; Datta, A.; Hazra, S. *Langmuir* **2005**, *21*, 5894.
(43) Ries, H. E., Jr. *Nature* **1979**, *281*, 287.

and the v-shaped geometry is favored. An approximation of this geometry is also depicted in Schemes 2 and 3, where the two hydrophobic nonyl chains are symmetrically repelled outward and the head group is in contact with the water surface. When comparing the behavior of **3** and **4** with that of the stearic acid complexes with divalent ions, a major difference is evident: In the latter case, both the ligand (protonated stearic acid) and the metal charges remain unchanged, with a M/L stoichiometry assumed constant as 1:2. As a result, the nature of the metal ion determines the surfactant geometry, and the collapse profile, as v-shaped for the smaller manganese(II) and cobalt(II) (constant pressure) or linear for the bulkier cadmium(II) and lead(II) ions (constant area). In this study, the ion is kept constant for **3** and **4**, but the nature of the ligand changes considerably. The same cobalt(II) ion seems to collapse at constant pressure for **3** and constant area for **4**, implying that the nature of the ligand is also instrumental in defining the mechanism of collapse.

The Brewster or polarization angle can be detected when the intensity of the vertical component of reflected polarized light passes through a minimum while moving between two media of dissimilar refractive index. Because agglomerates, domains, and monolayers differ in refractive index from the surrounding area, visualization of bidimensional structures in films becomes possible. Brewster angle microscopy (BAM) was used in the films of **3** and **4** in an attempt to investigate these two possible collapse mechanisms. Figure 7 shows a series of BAM micrographs for both complexes.

Careful analysis of the micrographs for **3** reveals that condensed domains of elongated shape are present before compression. At around 10 $mN{\cdot}m^{-1}$, hence before the first inflection, a smooth film is observed and was interpreted as the formation of a monolayer. At around 23 $mN{\cdot}m^{-1}$, thus close to the second inflection, condensed domains are observed again, and we interpret that as an indication that the monolayer has collapsed after the first inflection. Because no drop in pressure was observed, it confirms the constant pressure mechanism. Domains of elongated shape are observed immediately after the second inflection ($\sim$28 $mN{\cdot}m^{-1}$), indicating further folding of the multilayer. It is noteworthy that a recent article on the patterns in domains of Langmuir monolayers shows comparable isotherm and micrographs for *N*-hexadecanoyl L-alanine on a zinc(II)-containing subphase.[44] Although the BAM data succeeds in diagnosing the presence of a collapsed multilayer, the study of the linear versus v-conformation molecular shapes cannot be attained by this technique. Similarly, the micrographs of **4** are in good agreement with the proposed constant-area collapse. Only minor aggregates were observed before compression, and a uniform monolayer was observed at 7 $mN{\cdot}m^{-1}$. Between 8−10 $mN{\cdot}m^{-1}$, coinciding with the inflection seen on the isotherm, a somewhat uneven and rough pattern can be observed. It was first considered as an indication of collapse, but as the compression moves to higher surface pressures (25 $mN{\cdot}m^{-1}$), a homogeneous film is observed. Therefore, we interpret the rough surface seen around 8−10 $mN{\cdot}m^{-1}$ as a mesophase that leads to some sort of reorganization of the monolayer. Collapse of the monolayer is clearly observed at ca. 65 $mN{\cdot}m^{-1}$.

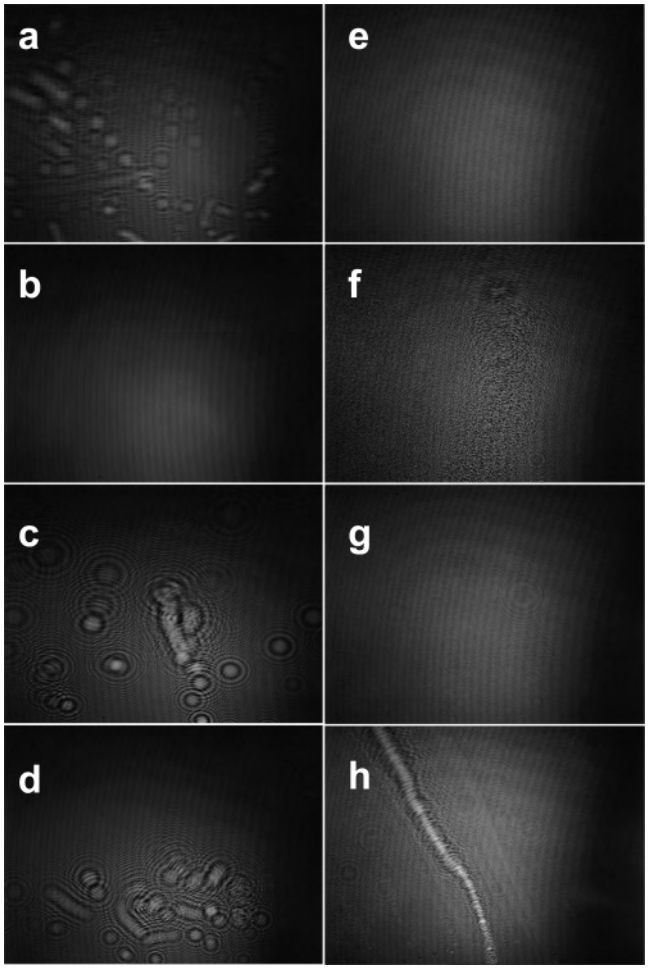

Figure 7. BAM micrographs for amphiphiles **3** (left) and **4** (right): (a) **3** before compression; (b) **3** at $\Pi = 10$ $mN{\cdot}m^{-1}$; (c) **3** at $\Pi = 23$ $mN{\cdot}m^{-1}$; (d) **3** at $\Pi = 28$ $mN{\cdot}m^{-1}$; (e) **4** at $\Pi = 7$ $mN{\cdot}m^{-1}$; (f) **4** at $\Pi \approx 8-10$ $mN{\cdot}m^{-1}$ (g) **4** at $\Pi = 25$ $mN{\cdot}m^{-1}$; (h) **4** at $\Pi = 65$ $mN{\cdot}m^{-1}$.

One can conclude that the coordination of bivalent cobalt to the deprotonated form of HL^{I-ODA} yielded **3**, which suggests the octadecyl fragment might be too long and flexible to support high collapse pressures and, consequently, highly packed Langmuir monolayers. The same reaction with the deprotonated form of HL^{I-NOBA} yielded **4**, a system of well-characterized structure that shows amphiphilic properties, good organization, and collapse pressure.

Equilibrium Contact Angles and Atomic Force Microscopy for the Langmuir−Blodgett Films of 3 and 4. Langmuir monolayers of **3** and **4** are readily transferred onto mica substrates. In an attempt to assess the nature of the films, we carried on depositions at 10 and 25 $mN{\cdot}m^{-1}$ for **3** and at 7 and 25 $mN{\cdot}m^{-1}$ for **4**, as indicated in Figure 6. Characterization of these films was performed via equilibrium contact angle (θ) and atomic force microscopy. The measurement of θ at which a liquid/air interface meets the solid surface is used as a quantitative measure of the wetting of a solid by a liquid[45] and helps determine whether a

(44) Hoffmann, F.; Stine, K. J.; Hühnerfuss *J. Phys. Chem. B* **2005**, *109*, 240.

monolayer has been transferred to a substrate by comparing the pre- and post-deposition angle formed by a drop of water on a given substrate. Whereas hydrophilic surfaces such as mica yield an effective $\theta \approx 0°$, highly hydrophobic surfaces present angles between 70 and 90°. The higher the θ value, the more hodrophobic the surface. Average values of 80 and 90° were observed for the films of **3** at 10 and 25 $mN \cdot m^{-1}$ respectively, whereas 91° was observed for **4** at 7 and 25 $mN \cdot m^{-1}$. In all of the cases, there is a sharp contrast between the θ value of the hydrophilic mica substrate and that of the hydrophobic LB films, suggesting that the polar head is in contact with the mica surface, whereas the hydrophobic chains point outward. It is interesting that the two films obtained for **4** present equivalent hydrophobicity, whereas those for **3** indicate an increase in hydrophobicity in moving from 10 to 25 $mN \cdot m^{-1}$. On the basis of the isotherm profiles, the BAM micrographs, and the differences in contact angles, it seems that a single monolayer is transferred for both LB films of **4**, whereas for **3** a monolayer is transferred only at 10 $mN \cdot m^{-1}$. Tapping mode AFM data was obtained for all of the LB films and revealed smooth surfaces. The inset in Figure 6 exemplifies the topography of the LB film for **4** at 7 $mN \cdot m^{-1}$. Unfortunately, several attempts to determine the thickness of the films by scratching their surface with the tip of the cantilever proved to be unsuccessful at this point.

Summary and Conclusions

We have observed that the iodo and bromo substituents in the phenolate group of asymmetric NN′O ligands stabilize cobalt(II) ions and yield the compounds $[Co^{II}(L^{IA})_2]$ (**1**) $[Co^{II}(L^{BrA})_2]$ (**2**). This was the starting point for the development of amphiphilic species based on the incorporation of OD and NOB functionalities to similar head groups. The cobalt(II) metallosurfactants $[Co^{II}(L^{I-ODA})_2]$ (**3**) and $[Co^{II}(L^{I-NOBA})_2]\cdot CH_2Cl_2$ (**4**) were isolated and studied. A crystal structure was obtained for **1** and showed a centrosymmetric pseudo-octahedral metal center surrounded by two facially coordinated ligands. The equivalent donor sets in both ligands are trans to each other, and the metal adopts a local D_{2h} symmetry that is favored by at least 2.3 $kcal \cdot mol^{-1}$ when compared to cis-coordinated isomers in a simplified model with nonsubstituted phenolate groups. Because this experimentally determined trans-phenolates geometry is the preferencial one, a correlation between the coordination sphere in archetype **1** and in amphiphiles **3** and **4** is proposed. The results for DFT calculations and EPR spectroscopy are in excellent agreement, indicating a high-spin $S = {}^3/_2$ electronic configuration given by $[a_g^1, b_{1g}^1, a_g^1, b_{2g}^2, b_{3g}^2]$ and located in pseudo-octahedral environments. This oxidation state was indirectly observed by the lack of counterion vibrations in the infrared spectrum and by the lack of a $p\pi_{phenolate} \rightarrow d\sigma^*_{cobalt(III)}$ charge-transfer band found between 430 and 470 nm for similar cobalt(III) species. The absence of the LMCT band observed for all of the species suggests that optical responsiveness can be attained by switching from cobalt(III) to cobalt(II), either via electrochemical or chemical stimuli. The electrochemistry of **1**−**4** is marked by metal-centered and ligand-centered activity. Regrettably, these oxidations and reductions lead to chemical side reactions and film formation, limiting the use of the amphiphiles as redox responsive materials. Both nonmetallated ligands and metallosurfactants are interfacially active. The McSMs **3** and **4** present different collapse mechanisms, leading to the formation of mono- or multilayers that depend on the nature of the ligand and the pressure by which Langmuir monolayers are deposited on mica. Surfactant **3** may adopt a v-shaped or a linear geometry, leading to a constant-pressure collapse mechanism that fosters the formation of multilayers. In the case of the more-rigid **4**, the v-shaped geometry is preferred, favoring a constant-area collapse and the formation of monolayers. Collapses and mono/multilayer formations were identified by Brewster angle microscopy. Deposition onto mica substrates yielded Langmuir−Blodgett films, as characterized by equilibrium contact angle and atomic force microscopy.

Therefore, one can onclude that the nature of the substituents in the phenol ring allows for the stabilization of a divalent cation but compromises the reversibility of the phenoxyl radical formed upon ligand oxidation. We have also shown that metallosurfactant **4** is prone to form ordered monolayers due to the presence of polar and more-rigid benzyloxy groups and shorter alkyl chains. The polar group might improve the submersion of the head group, whereas the short tails may prevent excessive disorder triggered by a linear geometry of the amphiphile. Current efforts involve the study of the influence of different transition-metal ions such as manganese, iron, nickel, copper, and zinc in the behavior of these amphiphiles. A thorough analysis of the Langmuir and LB films is also planned.

Acknowledgment. C.N.V. thanks Wayne State University, the Donors of the ACS-Petroleum Research Fund (Grant 42575-G3), the Nano@Wayne initiative (Fund-11E420), and the National Science Foundation (Grant CHE-0718470), and S.R.P.R. thanks the National Science Foundation (Grant CBET-0553537) for financial support. R.S. acknowledges the receipt of a Graduate Research Assistantship from the WSU-Institute for Manufacturing Research. Computer time allocated at the WSU-Grid System to the DFT calculations is also acknowledged.

Supporting Information Available: Cartesian coordinates and energies of optimized structures and crystal structures in CIF format. This material is available free of charge via the Internet at http://pubs.acs.org.

IC7011815

(45) de Gennes, P. G. *Rev. Mod. Phys.* **1985**, *57*, 827 − 863.